LRP 639/99 July 1999

Optical Diagnostics for Plasma Density Fluctuations

H. Weisen

ISSN 0458-5895

Optical diagnostics for plasma density fluctuations

Henri Weisen

Centre de Recherches en Physique des Plasmas

Association Suisse-Confédération Suisse

Ecole Polytechnique Fédérale de Lausanne

CH-1015 Lausanne, Switzerland

English language preprint of a textbook chapter for

Experimental methods of plasma diagnostics

V. I. Davydenko, A. A.Ivanov and H. Weisen
(in Russian)

edited by Alexander A. Ivanov
Budker Institute of Nuclear Physics
Novosibirsk

to be published September 1999 by
Novosibirsk University, Publishing Department
630090, Novosibirsk, ul.Pirogova 2, Russia

July 9th, 1999

Contents

Optical diagnostics for plasma density fluctuations

1) Wave propagation through inhomogeneous refractive media

Fundamentally the interaction of electromagnetic waves with a material medium such as a plasma a scatterig process, by which incident radiation is scattered by a collection of particles. In the case of plasmas the relevant process is Thomson scattering from free electrons. The scattered light not only conveys information on the random motion of the particles (incoherent scattering), but also on their collective motion and spatial distribution properties at scales which can far exceed the Debye length (coherent scattering). In the latter case it is usually simpler to consider the plasma as a continuous medium characterised by its dielectric properties. The connection between the continuous medium approach and the scattering description is given by the forward scattering theorem which provides a relation between the dielectric constant and the forward scattering amplitude (Jackson, 1975 sect. 9.14).

1.1 Diffraction

In this chapter we shall consider diagnostics for plasma phenomena such as microturbulence and plasma waves which have spatial scales of the order of the ion Larmor radius or larger and frequencies well below those of the optical frequencies used to probe them. When the probe beam frequencies are sufficiently larger than any important charcteristic plasma frequency, such as the electron cyclotron frequency, we may consider the plasma as a refractive medium with a refractive index given as

$n = \sqrt{1-\omega_{pe}^2/\omega^2}$ (eq.1), where $\omega_{pe}^2 = \frac{e^2 n_e}{\varepsilon_0 m_e}$ is the plasma frequency.

For $\omega^2 >> \omega_{pe}^2$, $n \cong 1-\omega_{pe}^2/2\omega^2$.

In the case of a monochromatic of wave number k_0 and frequency ω_0 in a quasi-stationary medium ($\partial n/(n-1)\partial t << \omega_0$), the propagation of the probe beam is governed by a wave equation of the form

$$\left(\nabla^2 + k_0^2\right)\underline{E} = -k_0^2\left(n^2-1\right)\underline{E}, \text{ (eq.2)}$$

where $\underline{E}$ is the electric field vector. Formally its solution may be expressed in the form of an integral equation (Jackson, 1975, sect. 6.6):

$$\underline{E}(\underline{r},t) = \underline{E}_0(\underline{r},t) + k_0^2 \int_{V'} \frac{\exp(ik_0|\underline{r}-\underline{r}'|)}{4\pi|\underline{r}-\underline{r}'|}\underline{E}(\underline{r}',t)\left[n^2(\underline{r}',t)-1\right]d^3\underline{r}'. \text{ (eq.3)}$$

In the case of weak interactions the effect of the refractive medium, quantified by $\underline{E}$-$\underline{E}_0$, on the incident wave field, may be approximated by assuming $\underline{E}(\underline{r}',t) \cong \underline{E}_0(\underline{r}',t)$ in the integrand of eq. 3. This is the well known Born approximation which is often implicitly assumed in the interpretation of scattering experiments.

We may further assume that the incident wave is a plane wave with wave vector $\underline{k}_0$. For $|\underline{r}| = R >> |\underline{r}'|$, the diffracted field $E_d = E - E_0$ can be written in the Born approximation as

$$\underline{E}_d(\underline{r},t) = \frac{k_0^2}{4\pi R}\int_{V'}\left[n^2(\underline{r}',t)-1\right]\exp(i\underline{k}\underline{r}')dV', \text{ (eq.4)}$$

where $\underline{k}=\underline{k}_d-\underline{k}_0$, and $\underline{k}_d=\underline{k}_0\underline{r}/R$ is the wave vector of the light scattered to the location $\underline{r}$. Eq. 4 shows that in the far field the diffracted field into the direction $\underline{k}_d$ is proportional to the Fourier transform of n^2-1 for the spatial frequency $\underline{k}$.

1.2 Geometrical optics

For strong interactions there is in general no simple approximation for eqs. 2 or 3. One particular one, corresponding to forward scattering, is however noteworthy, since it corresponds to the approximation of geometrical optics. It may be obtained by ignoring the vector nature of the field amplitude, using the Ansatz $E(\underline{r})=\exp(\rho+i\phi(\underline{r}))$, where ρ and ϕ are real functions, to obtain a solution of the wave equation (Rytov transformation). It is easily shown that the real and imaginary parts of the wave equation can be written as

$(\nabla\phi)^2 = k_0^2 n^2 + \nabla^2\rho + (\nabla\rho)^2$ (eq.5) and $\nabla^2\phi = -2\nabla\phi\nabla\rho$ (eq.6).

For media which are homogenous at a scale greater than the probe wavelength, the RHS second and third terms of eq. 5 can be neglected, yielding the eikonal equation of geometrical optics. This equation defines rays which at every point in space are parallel to $\nabla\phi$ and perpendicular to the wavefronts defined by ϕ=constant. The solution of the eikonal equation is obtained as

$\phi(\underline{r}) - \phi(\underline{r}_0) = k_0 \int_{\underline{r}_0}^{\underline{r}} n(l)dl$, (eq.7), where the line integral is evaluated along a ray.

The field amplitude is obtained using equation 6, $\Delta\rho(\underline{r}) = \rho(\underline{r}) - \rho(\underline{r}_0) = -\frac{-1}{2k_0}\int_{\underline{r}_0}^{\underline{r}} \frac{\nabla^2\phi}{n} dl$ (eq.8)

and back-transforming: $|E(\underline{r})| = \exp\left\{\frac{-1}{2k_0}\int_{\underline{r}_0}^{\underline{r}} \frac{\nabla^2\phi}{n} dl\right\} |E(\underline{r}_0)|$ (eq.9).

In most practical applications it is desirable that the amplitude be approximately constant and rays be nearly straight. This can be seen to be the case when $L \cong |\underline{r}-\underline{r}_0| \ll 1/|\nabla n/n|$.

1.3 Thin phase objects

A comparison of equation 8 with equations 3 or 4 shows that diffraction phenomena are beyond the scope of geometrical optics. Paradoxically, many experimental situations can be described using combinations of both the diffraction theory and geometrical optics. For this reason we need to investigate the conditions for which we may apply geometrical optics in media where diffraction is known to occur. In general we'll be interested in small refractive index changes expressed as $n=1+n^*$, where $|n^*|$ can be arbitrarily small. The corresponding amplitude changes, estimated from equation 7 and 8, are of order $\rho \sim k^2L^2|n^*|/4$, where k is the wavenumber of the refractive perturbation of interest . Considering the terms neglected in the derivation of the eikonal equation (eq. 5), the most stringent condition is obtained by requiring $|\nabla^2\rho| = k^2\rho \ll k_0^2\Delta n^2 \cong 2\, k_0^2|n^*|$, or, introducing the wavelengths of the incident radiation $\lambda=2\pi/k_0$ and the refractive perturbation, $\Lambda=2\pi/k$:

$L^2 << \Lambda^4 / \lambda^2$ (near field condition, inequality 10).

The condition is pictured on fig.1, showing a plane wave incident onto a refractive medium in a slab of thickness L, with transverse perturbations of scale Λ. These scatter radiation at angles $\pm\lambda/\Lambda$ corresponding to the orders of diffraction ± 1. Inequality 10 is equivalent to stating that the diffracted waves must have diverged by much less than a distance equal to Λ from the incident wave on exiting the slab.

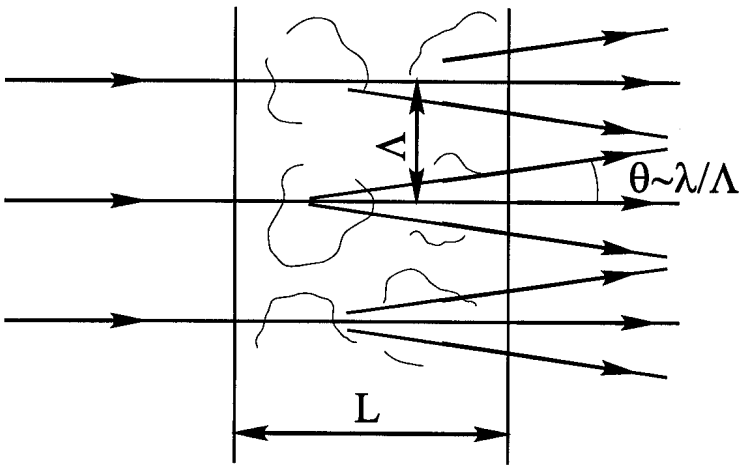

Fig.1 Diffraction by a slab with refractive perturbations

Fig. 2 illustrates the wavenumber matching condition $\underline{k}_{\pm 1}=\underline{k}_0\pm\underline{k}$. Since we only consider low frequency perturbations, $\omega_{\pm 1}=\omega_0\pm\omega\cong\omega_0$, we must require $|\underline{k}_{\pm 1}|\cong|\underline{k}_0|$ corresponding to the Bragg relation, $\sin(\theta/2)=k_0/2k$. Permissible scattered wave vector lie on the circle in the figure. We may now note that for an interaction volume of finite depth L, the wavevector of the perturbation is only defined within $\Delta k_z\approx 1/L$. From this we may distinguish two regimes depending on whether or not the Bragg relation can be simultanously satisfied for both orders +1 and −1. As seen from fig.2 the regime of simultaneous diffraction in both orders corresponds to $\Delta k_z >> k^2/k_0$ which is equivalent to inequality 10. This regime is also referred to as Raman-Nath diffraction and refractive media satisfying the near field condition are called 'thin'.

Hence over short enough distances we may use geometric optics to describe wave propagation. In many cases of small-angle scattering the interaction volume may be small enough for describing the interaction using the eikonal equation, whereas the detection apparatus may be in the far field where geometrical optics fails.

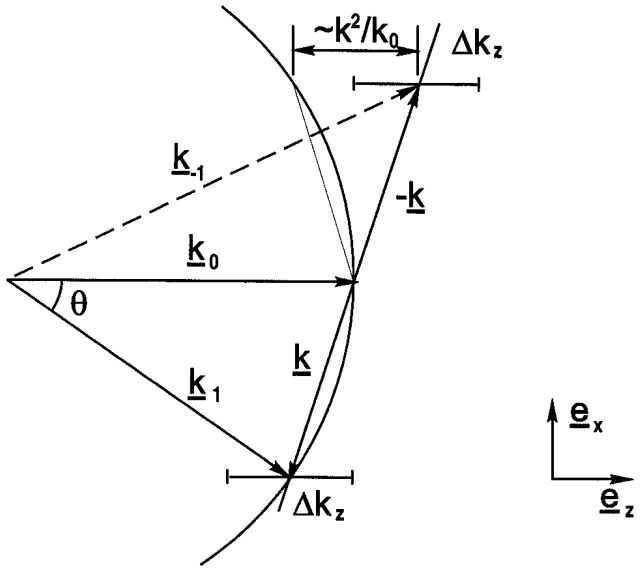

Fig.2 The wavenumber matching condition

2) Collective scattering diagnostics

A typical arrangement for scattering from refractive perturbations in a plasma is shown in fig. 3. It involves a probing beam, typically a coherent Gaussian beam from a laser or a microwave source. In principle scattered radiation could be collected by just viewing the incident beam with a suitable lens and detector. In general however scattered field amplitudes are extremely small and require heterodyne (or homodyne) detection shemes. For this purpose the scattered radiation is made to interfere with a local oscillator. The local oscillator can be provided by a second source, often at a slightly different frequency (heterodyne detection), or by splitting off a fraction of the source radiation (homodyne detection). In one common sheme the local oscillator crosses the probe beam inside the plasma, although this leads to a drop in responsivity for $|\underline{k}|<1/w$, where w is the beam width (see exercises). The intersection of the two beams defines the scattering volume. The local oscillator may also be introduced using a beam splitter after the scattered radiation has left the plasma (dashed lines in fig.3). In this case there is no lower limit to the wavenumber response; the instrument functions as an interferometer for $|\underline{k}|=0$. The resulting power density on the detector can be written (up to a factor ε_0) as

$$I = |E_d + E_{lo}|^2 = |E_d|^2 + |E_{lo}|^2 + E_d E_{lo}^* + E_d^* E_{lo}, \text{ (eq.11)}$$

where *lo* designates the local oscillator field and * denotes a complex conjugate. The detector size is chosen as to intercept all of the local oscillator and scattered radiation, corresponding to a detectable power given by:

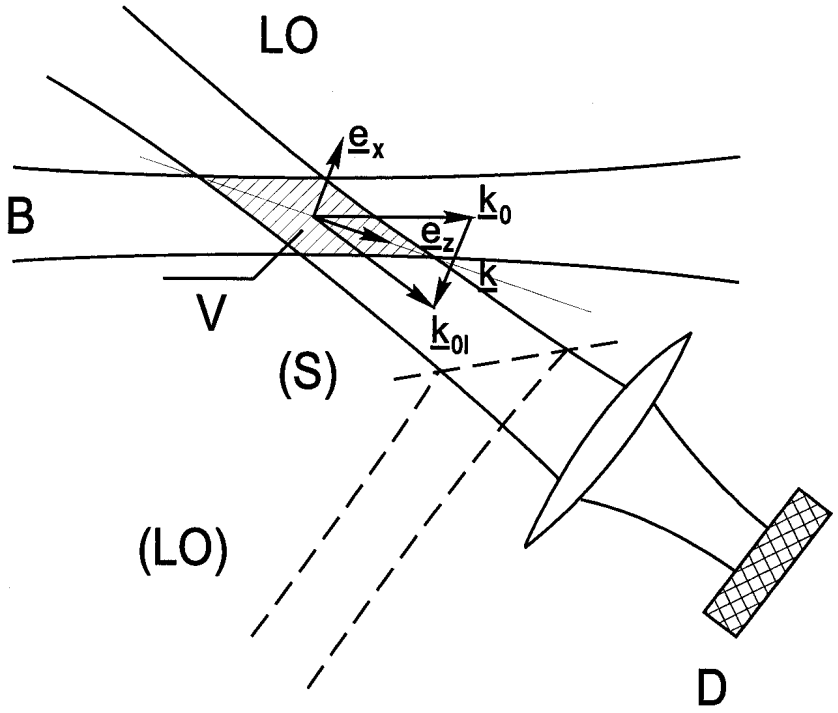

Fig.3 Typical scattering geometry for heterodyne detection. B incident beam, LO local oscillator, V scattering volume, S beam splitter, D detector.

$$P = \int \left(E_d E_{lo}^* + E_d^* E_{lo} \right) dS \quad \text{(eq.12)}$$

Equation 12 has the form of a scalar product and means that the detected power will be proportional to the projection (in the functional sense) of the scattered field onto the local oscillator field. This scalar product is conserved during propagation and may be evaluated anywhere along the local oscillator beam. This explains the high selectivity of heterodyne methods. Radiation not originating from within the portion of space defined by the local oscillator beam, or not propagating in the direction $\underline{k}_{0l}$ defined by the local oscillator, does not contribute to the signal. From eq.4 we see that the detected power is proportional to the spectral power density in wavenumber space of the electron density fluctuations evaluated at $\underline{k}=\underline{k}_d-\underline{k}_0$. For a density perturbation of the form of a plane wave, $\tilde{n}_e = \tilde{n}_{e0}\cos(kr - \omega t)$, satisfying the Bragg relation, the scattered power from within the observation volume can also be expressed as $P_s = \tilde{n}_{e\,0}^2 P_i r_e^2 \lambda^2 l^2 / 4$, where l is the length of the interaction volume along the probe beam, P_i its power and $r_e=e^2/(4\pi\varepsilon_0 m_e c^2)$ is the classical electron radius. Using an array of detectors it is possible to reconstruct all, or a significant portion, of the fluctuation spectrum. A multichannel scattering diagnostic, using an optically pumped far infrared laser, has for instance been used on the TEXT tokamak (Brower et al. 1985,1987, fig.4). This experiment used two coherent far infrared lasers with λ=1.222mm which were optically pumped by a CO_2 laser. The probe and local oscillator lasers were actively feedback-tuned in order to achieve heterodyne detection with a stable intermediate frequency of 1 MHz, permitting a Doppler measurement of the direction of propagation of low frequency drift waves. The entire optical setup was moveable in the vertical and horizontal

directions, which allowed the characteristics of plasma turbulence to be mapped out for the entire plasma cross section.

For probe and l.o. fields with Gaussian profiles the product of the spatial and wavenumber resolutions, $\Delta k \Delta x$ is minimum. The wavenumber resolutions are given by

$$\Delta k_y/k=\Delta k_x/k=2/\pi r \text{ and } \Delta k_z/k=k/(\pi k_0 r), \text{ (eq.13)}$$

where $r=wk/\pi=2w/\Lambda$ (Holzhauer and Massig, 1978).The Gaussian beam half-width w of the incident and l.o. beams is defined at the 1/e points of the beam intensity and similarly $\Delta k_{x,y}$ are defined at the 1/e points of the power spectrum of the l.o. beam. The length of the interaction volume along the direction z is given by $l=2w\Lambda/\lambda=r\Lambda^2/\lambda$. (eq.14)

The choice of a probing wavelength and scattering arrangements is often a compromise between the desire for spatial resolution, expressed as $l \ll L$, where L is the plasma size and the desire for wavenumber resolution. For many types of fluctuations of interest in high temperature plasmas scattering angles are too small to achieve spatial resolution along the direction of propagation.

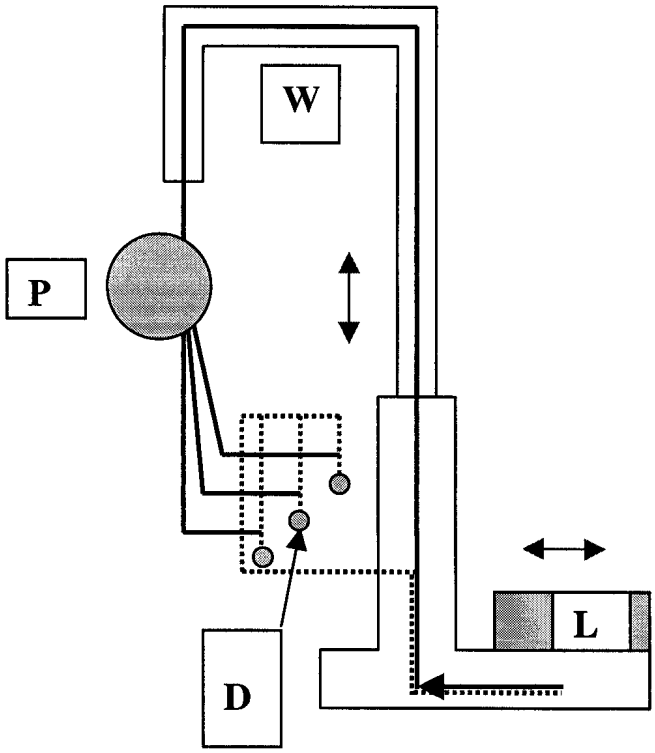

Fig.4 Multi-channel scattering diagnostic on the TEXT tokamak (adapted from Brower et al 1985). P plasma, W dielectric waveguide, L infrared laser sources, D detectors. Probe beam is shown as continuous line, local oscillator is broken line. Only 3 out of 6 channels are shown, beam splitters and mirrors are not shown for simplicity.

Scattering diagnostics have been used extensively to study drift wave turbulence in high temperature plasmas, and to a lesser extent externally excited plasma waves. Radiation sources vary from millimeter wave sources (Mazzucato 1976, Equipe TFR 1983) such as klystrons through far infrared lasers (Brower et al 1985,1987) to CO2 lasers emitting in the mid-infrared (Slusher and Surko, 1980, TFR Group and Truc, 1984). Consequently detection shemes involve (sub)millimeter diode mixers or liquid nitrogen cooled infrared photoamperic diodes.

3) Transmission methods

Transmission methods are mostly used for measuring macroscopic parameters such as the density profile through interferometry. These may involve several discrete beams passing through the plasma at different locations (Véron, 1979) or, if large ports and windows are available, a single wide probe beam encompassing all or most of a plasma cross section (Hugenholtz and Meddens 1982, Young et al, 1985). In the latter case the plasma is either imaged onto a multi-element detector or the detector is in the near field of the interaction region defined by inequality 10. A schematic of an imaging Mach-Zehnder interferometer is shown in fig.5. Although interferometry may be considered the queen of transmission methods, an astounding variety of imaging and near field methods has been developed for investigating various refractive media as occur in transmission microscopy, wind tunnel experiments and plasma physics (Wolter, 1956, Vasil'ev 1971, Jahoda 1971). These methods usually emphasize regions of particular interest such as regions of strong gradients or regions which scatter light and have the advantage of being considerably less sensitive to vibrations than interferometers. These methods all qualify as spatial filtering methods although their interpretation depends on the regime of interaction of the probe radiation with the refractive medium. In many early experiments plasmas were much smaller and denser than those of today's fusion research devices and could be studied using visible lasers such as the pulsed ruby laser, using photographic film as a detector.

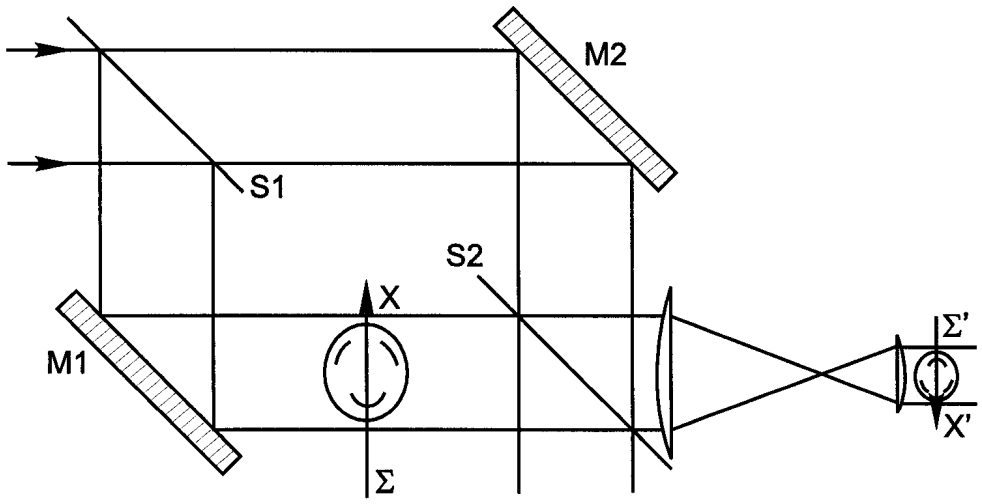

Fig.5 Mach-Zehnder imaging interferometer. S1, S2, beam splitters, M1,M2, mirrors, Σ,Σ', object and image planes.

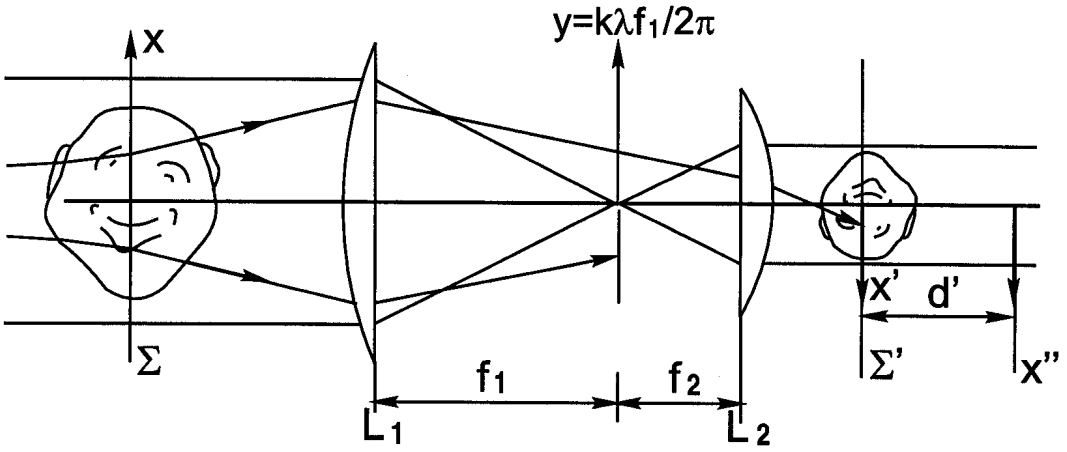

Fig.6. Schlieren setup with knife edge spatial filter. The instrument can work in shadowgraphy mode without a spatial filter if the object is displaced form Σ by a distance -d or if the detection is displaced to plane Σ'' by a distance d'=$f_2 d/f_1$.

A classic example is the knife-edge Schlieren method (fig.6) due to Foucault, who used it for the testing of astronomical mirrors. In the geometrical optics description refractive index gradients produce changes in the direction of light propagation which are given by

$$\alpha(x,y) = k_0 \nabla_\perp \phi(x,y) \quad \text{(eq. 15)}$$

where ϕ is given by the line integral of eq.7. In the setup of fig.6 the refractive object is illuminated by parallel light and situated in the object plane Σ of the telescope formed by lenses L1 and L2. The detector array or photographic plate is in the image plane Σ'. The effect of the knife edge is to stop light with propagation angles below a threshold given by its position in the focus of L1, from reaching Σ'. In this case the image will only show those regions of the phase object which produce transverse phase gradients exceeding a set value. If the illumination is produced by an extended source, every region in the object plane will produce an image of in the focal plane of L1. Since the displacement of this image depends on the deflection angle so will the amount of light contributing to the image of the phase object in Σ'. Hence the intensity in the image is proportional to the line integrated transverse gradient of the refractive index. Numerous variants exist depending on the nature of the filtering and illumination. A simple variation, called shadowgraphy, uses no filter, but instead produces intensity modulations by means of out-of-focus imaging. From eq. 9 we see that if the object is out of focus by a distance z, it produces intensity modulations given to first order by

$$\frac{\Delta I(x,y)}{I_0} = \frac{-z\nabla_\perp^2 \phi(x,y)}{nk_0}. \quad \text{(eq. 16)}$$

Since the Schlieren methods consist of simultaneous measurements of transverse wavenumber and position, they are, just as scattering methods, limited by the uncertainty principle to $\Delta(\nabla_\perp\phi)\Delta x,y \geq 2\pi$. The relatively small phase shifts and phase gradients produced by high temperature plasmas in magnetically confined fusion research preclude the use of geometrical optics based Schlieren methods in those media. In fact, geometrical optics predicts vanishingly small deflection angles for plasma density fluctuations of vanishingly small amplitude, whereas the diffraction

integrals (eqs. 3 and 4) show that the diffraction angle depends solely on the wavenumber k of the fluctuations considered, not however, on their amplitudes. In this context, optical filtering methods cannot be interpreted in terms of geometrical optics, even though there are striking instrumental similarities between Schlieren methods and wave-optics based filtering techniques.

Optical filtering offers attractive alternatives to the more traditional scattering techniques in the case of perturbations with spatial scales such that the plasma is optically thin in the sense of equation 10. When comparing the various methods it should be kept in mind that the diffracted light carries away a certain amount of information about the fluctuations in the plasma, namely about the fraction of the fluctuation spectrum which satisfies the Bragg condition. It is up to the skills of the diagnostic designer to extract as much of this information as possible, although the form in which the information is extracted may differ and require specific interpretation. The essential difference between imaging and scattering diagnostics is that the former provide a real-space representation of the fluctuations whilst the latter provide a wavenumber spectrum. Clearly, if all of the diffracted amplitude is measured, both approaches are equivalent and provide all of the information that can be extracted from the diffracted wavefield. Depending on whether the fluctuations of interest are spatially homogenous or not, one or the other approach may provide more directly interpretable information.

The most accomplished of the wave optics based filtering methods is the phase contrast method, for which Zernike was awarded the 1935 Nobel prize (Zernike 1934, 1935). This method is used to detect weak phase perturbations ($\phi<<1$) and produces intensity modulations which are directly proportional to ϕ. The phase contrast method was originally invented for the microscopic visualization of living organisms whithout the need to stain them and later also applied electron microscopy (Thon 1971) and to low mass density aerodynamic flows (Philbert 1964, Veret 1970). One group (Presby and Finkelstein, 1967) used it to study turbulent perturbations in high density plasmas using a pulsed ruby laser and photographic film for recording. These authors however appear not to have been fully aware of linear transfer properties of their filter setup, which only permitted the visualization of perturbations with wavelengths smaller than about 1mm. The phase contrast method has since been applied to study density fluctuations in the plasmas of the TCA tokamak (Weisen 1988), the DIII-D tokamak (S.Coda and M. Porkolab, 1995) and the C-MOD tokamak using wide probe beams produced by CO2 lasers (λ=10.6μm) and multi-element photoamperic detectors.

4) Optical filtering methods for weakly refractive media

4.1 Detection of small phase shifts.

Lets consider the case of a plane wavefront with a complex amplitude profile described by $B(\underline{x})$. It's interaction with a thin phase object may described by a multiplication with the eikonal phase factor (eq. 7):

$$B'(\underline{x},t) = \exp(i\phi(\underline{x},t))B(\underline{x}) \cong (1+i\phi(\underline{x},t))B(\underline{x}) \text{ for } \phi<<1. \text{ (eq.17)}$$

For simplicity we'll drop the time dependence and the vector notation for the position x. The intensity, $|B'|^2$, of the transmitted beam is unaffected by the transmission through a thin phase object (fig7a). In order to obtain a detectable change in intensity (power density) we need to add a wavefield that can

constructively interfere with the diffracted field iϕ(x), for instance by adding a reference wave of amplitude iB(x). This can be done using an interferometer such as shown in fig.5. The total wave field then becomes

$$B''(x) = B(x) + i\phi(x)B(x) + iB(x) \text{ and } I(x) = |B''(x)|^2 = 2|B|^2(x)(1+\phi(x)) \text{ (eq. 18)}$$

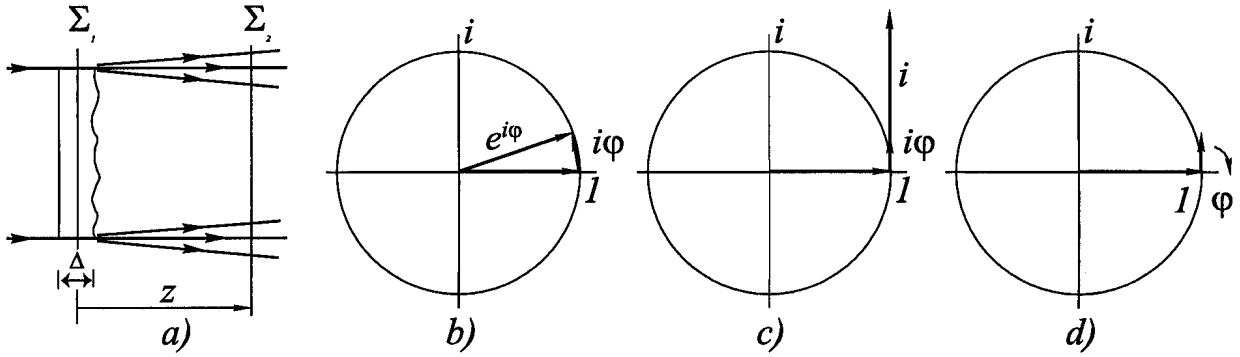

Fig 7. Detection of small phase shifts.

a) Transmission through a thin phase object

b) Phase relation of diffracted (iϕ) and undiffracted (1) components

c) Measurement of diffracted component by adding a reference wave (interferometry)

d) Measurement of diffracted component by phase-shifting (internal reference)

The relations between the complex amplitudes are shown in fig.7b and c. Other methods use no external reference. How do they manage to produce detectable intensity modulations? The answer is that, in a way or another, they derive a reference from within the transmitted beam (Weisen 1986). In the case of filtering techniques the different components of the wavenumber spectrum can be acted upon independently in the focus of lens L1. In the case of phase contrast (fig.8) the diffracted wavefield is phase-shifted by -π/2 (or +π/2) with respect to the transmitted beam. This leads to

$$B''(x) = B(x) + \phi(x)B(x) \text{ and } I(x) = |B''(x)|^2 = |B|^2(x)(1+2\phi(x)) \text{ (eq. 19)}$$

Other techniques can be understood similarly, although the phase shifts obtained are not necessarily the ideal ∓π/2 for all wavenumbers in the spectrum. Clearly no internal reference instrument can measure absolute phase changes as does an interferometer. It can only provide a phase relative to a weighted average of phases in the beam. This leads us to consider the linear transfer properties of optical filtering methods. The basic concepts of linear optical systems can be found in many textbooks (Gaskill, 1978) and will be introduced as we proceed.

The effect of an optical system on optical wavefields is described by a linear operation L, which provides the complex wavefields in the image field, knowing those in the object plane:

$$\begin{aligned} &L: B'(x) \rightarrow B''(x) = R(x) + D(x) \\ &L: B(x) \rightarrow R(x) \\ &L: i\phi(x)B(x) \rightarrow D(x) \\ &L: \delta(x-y) \rightarrow h(x,y) \end{aligned} \qquad \text{(eq. 20)}$$

where R(x) is the reference field and D(x) the diffracted field which is linear in ϕ. The linear transformation of the optical wavefields is often described by the impulse response h(x,y). If h(x,y)=h(x-y) the system is said to be shift invariant and may be characterized by its transfer function H(k), which is the Fourier transform of h(x). The intensity in the image plane is

$$I(x) = |R|^2(x) + R^*(x)D(x) + R(x)D^*(x) + |D|^2(x) \text{ .(eq.21)}$$

When $\phi << 1$, $|R|^2$ is the dominant term, the interference terms being of order $\phi|R|^2$ and the diffracted intensity a negligible $\phi^2|R|^2$. What we are interested in, is the linear relationship between $\phi(x)$ and the interference terms in the intensity. We may describe it by another linear operation which characterizes the optical instrument:

$$L_i : \phi(x) \rightarrow \Delta I(x) \text{ where}$$

$$\Delta I(x) = R^*(x)D(x) + R(x)D^*(x) \text{ (eq.22).}$$

This linear relation between $\phi(x)$ and $\Delta I(x)$ is described by the corresponding instrumental impulse response $h_i(x,y)$ which is the response $\Delta I(x)$ for a phase perturbation of the form of a delta function and is obtained by replacing $\phi(x)$ by $\delta(x-y)$ in equation 22. This impulse response has the general meaning of a transfer matrix when discretized, and may be inverted in order to reconstruct $\phi(x)$ from $\Delta I(x)$, provided it is well enough conditionned. The Fourier transform of $h_i(x,x-y)$ with respect to the variable u=x-y, for a fixed value of x, is a wavenumber response. We call it the instrumental transfer function $H_i(k)$ if the system is shift-invariant, i.e. if $h_i(x,y)=h_i(x-y)$. The impulse response and transfer function for the instrument as a whole (eq.22) and those pertaining to the optical wavefields (eq.20) must not be confused. Most optical systems are fairly shift-invariant within the image field and the transfer function yields an excellent basis for comparison of the various imaging methods. In the following sections we shall compute the terms of eq.22 for three imaging methods of interest. Before doing so, we imagine that we use the same illumination source and magnification for a Mach-Zehnder imaging interferometer as shown in fig.5. From eq. 18 we see that $\Delta I=\phi I$, where I is the intensity in the output arm of the interferometer. The necessity of splitting the beam leads to $I=I_0/2$, $I_0=|B|^2$ being the intensity available for non-interferometric methods using the same source. Hence for the interferometer we can write

$$\Delta I = I_0 \cdot \phi/2, \text{ hence } h_i(u) = \delta(u)/2 \text{ and } H_i(k) = 1/2 .$$

These functions are shown in fig.11a, a' and will serve as a comparison for those pertaining to the methods discussed below.

4.2 Phase contrast

An example of a phase contrast setup is shown on figure 8. Using a telescope arrangement of two lenses of focal lengths f_1 and f_2 it produces a filtered image of magnification f_2/f_1 of the thin phase object placed at the plane Σ at the plane Σ'. The phase object is illuminated with a suitably expanded beam of parallel light from a source such as a laser. The spatial Fourier spectrum of the transmitted wavefield is mapped onto the focal plane the lens L1. It can be shown that for an ideal lens the wavefields in Σ and in the focal plane of L1 form an exact Fourier transform pair (Gaskill 1978) if their distance to L1 is equal to its focal length f_1. In practice however Σ may be essentially at any finite distance from L1, in which case the wavefield in the focus of L1 remains, up to an unimportant phase factor, the Fourier transform of the wavefield in Σ. Any spatial frequency (or wavenumber) component contained in the transmitted field propagates at an angle k/k_0 and hence appears at a position given by $x_k=k\lambda f_1/2\pi$. This 'Fourier plane' is equipped with a spatial filter called a phase plate which may

consist of a glass plate which is slightly thicker for $|k|>k_c$. The difference in thickness is adjusted such as to phase-shift diffracted light with $|k|>k_c$ by $-\pi/2$. Lens L2 produces a Fourier transform of this filtered spectrum, which is equivalent, up to an image inversion and a magnification factor, to a Fourier back-transformation. The image plane is equipped with suitable light-sensitive detectors such as an array of photoamperic diodes or a charge-coupled device (CCD). In a practical situation the system magnification f_2/f_1 is chosen such as to match the size of the image of the phase object to that of the detector array. In the following analysis of the transfer properties of this systems we shall assume a magnification equal to unity.

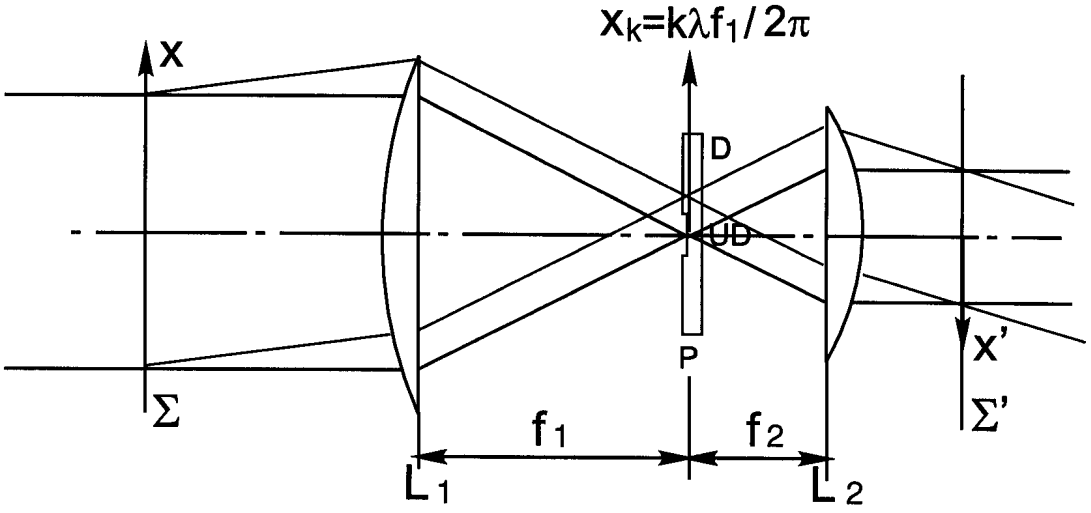

Fig 8. Optical setup for phase contrast. Σ object plane, Σ' image plane, L1,L2 lenses, P phase plate, D diffracted wave component, UD undiffracted wave component

The transmitted beam in plane Σ may be written as:

$$B'(x) = \{1 + i\phi(x)\}B(x) \text{ (eq. 23)}$$

where B(x) is the incident beam. In the Fourier plane the wave amplitude is

$$\tilde{B}'(k) = \{\delta(k) + i\tilde{\phi}(k)\} \otimes \tilde{B}(k) \text{ (eq. 24)}$$

where ~ designates the Fourier transform (FT) and ⊗ denotes the convolution operation defined by $a(k) \otimes b(k) = \int a(\xi)b(k-\xi)d\xi$. To obtain eq.24 we have used the convolution theorem, which states that the FT of a product of functions is the convolution of the FT's of these functions. The effect of the phase plate is described by

$$\tilde{B}''(k) = \{1 - (1-i)\tilde{C}(k)\}\tilde{B}'(k) \text{ ,(eq.25),}$$

where $\tilde{C}(k) = 1$ for $|k| \le k_c$ and $\tilde{C}(k) = 0$ for $|k| > k_c$.

The relevant quantities in the Fourier plane are shown in fig.9. If we wanted to take into account a finite optical resolution we would also have to specify here that $\tilde{B}''(k)$ drops to zero above some maximum value of |k|. In practical situations, for extended objects such as plasmas, this is likely to correspond to wavenumber for which the object is no longer thin in the sense of inequality 10 and phase contrast not a recommended diagnostic. Also the resolution is often limited by the available

detectors rather than by the optical properties of the system. For simplicity we shall therefore assume that there is no upper bound for the wavenumbers that can pass the optical system.

The wave amplitude amplitude distribution in the image plane is obtained by an FT back-transform:

$$B''(x) = R(x) + D(x)\,, \text{(eq.26)}$$

where

$$R(x) = B(x) + (i-1)B(x) \otimes C(x)$$

$$D(x) = i\phi(x)B(x) - (1+i)\{\phi(x)B(x) \otimes C(x)\}$$

and $C(x)$ is the inverse FT of $\tilde{C}(k)$. The corresponding intensity is given by eq.21. The interference terms (eq.22) are:

$$\begin{aligned}\Delta I(x) &= \left\{[B(x) \otimes C(x)]B^*(x)\phi(x) - B(x)[C(x) \otimes B^*(x)\phi(x)]\right\} + c.c. \\ &= 2B(x)\{[B(x) \otimes C(x)]\phi(x) - C(x) \otimes [B(x)\phi(x)]\} \qquad \text{(eq. 27)} \\ &= 2B(x)\left\{\int B(y)C(y-x)dy\phi(x) - \int C(y-x)B(y)\phi(y)dy\right\}\end{aligned}$$

From the above equation we see that ΔI(x) is proportional to the difference between φ(x) and a weighted average of φ over the neighbourhood of x. The impulse response is obtained by setting φ(x)=δ(x-y):

$$h_i(x,y) = 2B(x)[B(x) \otimes C(x)]\left\{\delta(x-y) - \frac{B(y)C(x-y)}{B(x) \otimes C(x)}\right\} \text{ (eq. 28)}$$

In the shift-invariant approximation (near y=0) this further simplifies to

$$h_i(x-y) = h(u) \cong 2I_0\left\{\delta(u) - \frac{B(-u)C(u)}{\int B(v)C(v)dv}\right\} \text{(eq.29).}$$

We have also used $B(x)[B(x) \otimes C(x)] \cong |B(x)|^2 = I_0(x)$. This approximation is justified if k_c is chosen large enough as not to substantially affect the incident beam. Finally the FT of $h_i(u)$ provides the transfer function:

$$H_i(k) \cong 2I_0\left\{1 - \frac{\tilde{B}(-k) \otimes \tilde{C}(k)}{\left[\tilde{B}(-l) \otimes \tilde{C}(l)\right]_{l=0}}\right\} \text{ (eq.30)}$$

The numerator is the correlation function of $\tilde{B}(k)$ and $\tilde{C}(k)$. As expected, we see that phase contrast cannot measure absolute phase shifts: $H_i(0)=0$. The transfer function is shown in fig.9 and the impulse response is shown on fig.11b'. The transfer function has a soft cutoff at $k=k_c$ and becomes wavenumber independent for higher wavenumbers. If k_c is chosen as to match the diffraction-limited spot size corresponding to B(x) the instrument is sensitive to perturbations with wavelength shorter than the beam width in the object plane. Its transfer function then comes close to that of a theoretically ideal internal reference interferometer (see exercises). Note that for $k>k_c$ the response is four times larger than for the interferometer shown in fig. 11a'.

In principle the system could be made arbitrarily sensitive by increasing the incident beam intensity I_0. In practice there are however power limits for the detectors. Photoamperic diodes used at CO_2 laser wavelengths (λ=10.6μm), for example, saturate for power densities larger than about 1mW/mm^2. This is rather modest considering the large powers (several tens of Watts) that can be obtained from standard laboratory CO_2 lasers. One can enhance the contrast by reducing the local

oscillator power in the image plane using a phase plate with a partly transmitting central region. The effect of a partly transmitting phase plate can be modelled by modifying eq.25 as follows:
$\tilde{B}''(k) = \{1 - \tilde{C}(k) + i\gamma\tilde{C}(k)\}\tilde{B}'(k)$ (eq.25b), where $\gamma \leq 1$ is the amplitude transmission factor. In this case the transfer function becomes

$$H_i(k) \cong 2\gamma I_0 \left\{1 - \frac{\tilde{B}(-k) \otimes \tilde{C}(k)}{\left[\tilde{B}(-l) \otimes \tilde{C}(l)\right]_{l=0}}\right\} \text{(eq.30b).}$$

The intensity due to the filtered incident radiation is approximately $\gamma^2 I_0$, hence for refractive perturbations with $k > k_c$ we obtain $\Delta I/I \cong 2\phi/\gamma$.

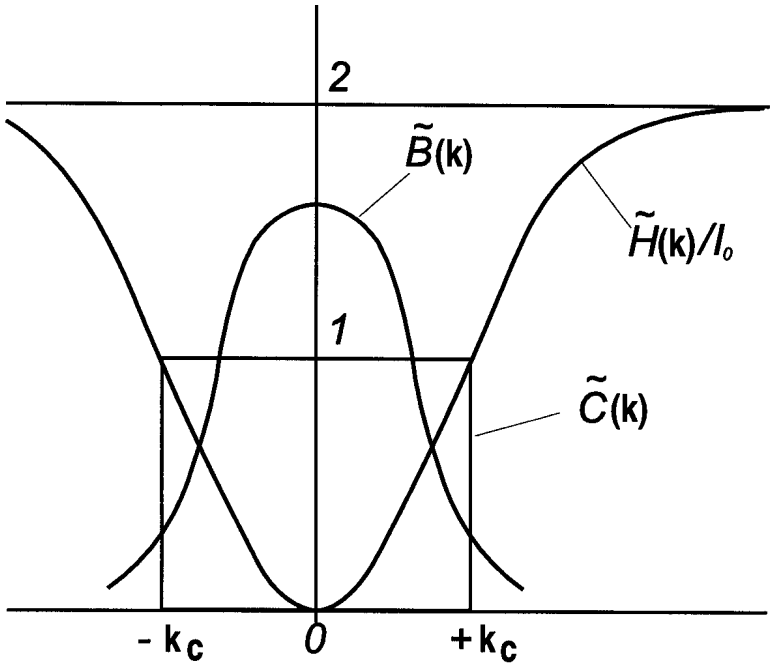

Fig 9. Fourier plane quantities and transfer function for phase contrast.

4.3 Scintillation

A very simple way of obtaining intensity variations as a result of phase variations is to position the detector a distance z behind the phase object, as sketched in fig.7a. A practical setup may still involve an imaging arrangement as shown in fig.8, but without the phase plate. The object is deliberately positioned out of focus by a distance z. In order to understand this method we need to calculate the transfer properties of free space propagation. The simplest is to consider monochromatic plane waves travelling from Σ_1 to Σ_2 as shown in fig.7a:
$E(x_1, x_2, z, t) = E_0 \exp i\{k_z z + k_{x1} + k_{x2} - \omega_0 t\}$, (eq.31),
with the relation $k_0^2 = k_z^2 + k_{x1}^2 + k_{x2}^2$.

Hence the transfer function describing the propagation from Σ_1 to Σ_2 is simply:

$$H_z(k_{x1}, k_{x2}) = \frac{E(x_1, x_2, z, t)}{E(x_1, x_2, 0, t)} = \exp ik_z z = \exp\left\{izk_0\sqrt{1 - \frac{k_{x1}^2 + k_{x2}^2}{k_0^2}}\right\}, \quad \text{(eq.32).}$$

A useful 2nd order approximation to eq.32, the Fresnel approximation, is obtained for propagation at small angles to the z-direction:

$$H_z(k) \cong \exp\left\{ik_0 z(1-\frac{k^2}{2k_0^2})\right\} \text{ (eq.33),}$$

In eq.33 we dropped the vector notation for (k_{x1},k_{x2}), although we still need to keep in mind that we are dealing with two-dimensional Fourier transforms. The corresponding impulse response, in the Fresnel approximation, is

$$h_z(x) \cong \frac{k_0}{2\pi}\frac{1}{iz}\exp\left\{ik_0 z(1+\frac{x^2}{2z^2})\right\} \text{ (eq.34).}$$

We may now calculate the intensity at a distance z from the phase object:

$$B''(x) = B'(x) \otimes h_z(x) = \{[1+i\phi(x)]B(x)\} \otimes h_z(x) \text{ . (eq.35)}$$

In the notation of equations 20-22:

$$R(x) = B(x) \otimes h_z(x) \text{ and } D(x) = i\phi(x)B(x) \otimes h_z(x) \text{ .}$$

The interference terms in the expression for the intensity are:

$$\Delta I(x) = -i\{B(x) \otimes h_z(x)\}\{[\phi(x)B^*(x)] \otimes h_z^*(x)\} + c.c.$$

The near field may be defined as the region close to the phase object where the modulus of the incident beam amplitude is not substantially changed: $B(x) \otimes h_z(x) \cong \exp(ik_0 z)B(x)$. With this definition, the instrumental impulse response can be approximated as:

$$h_i(x,y) \cong -\frac{k_0}{\pi z}B(x)B^*(y)\cos\left\{k_0\frac{(x-y)^2}{2z}\right\} \text{ (eq.35),}$$

or, in the shift invariant approximation ($B(x) \cong B(y)$, fig 11c),

$$h_i(u) \cong \frac{-k_0}{\pi z}I_0\cos\left\{\frac{k_0 u^2}{2z}\right\} \text{ (eq.36) and its two-dimensional Fourier Transform:}$$

$$H_i(k) \cong -2I_0\sin\left\{\frac{zk^2}{2k_0}\right\} \text{ (eq.37).}$$

This transfer function has a very oscillatory character, as shown on fig. 11c', which makes out-of-focus measurements difficult to interpret. Also, since the magnitude of the transfer function is reduced for most wavenumbers, part of the information in the transmitted wavefield is lost. We may note that for $k^2<|2k_0/z|$, where $H_i(k) \cong -I_0 z k^2/k_0$, the intensity distribution is proportional to the Laplacian $\partial^2\phi/\partial x^2$, just as in the case shadowgraphy in geometrical optics (eq.16). The Fresnel propagator $h_z(x)$ is also useful for evaluating the effect of defocussing on other methods and it is a very convenient tool for describing the propagation of Gaussian beams.

4.4 Knife edge and phase blade spatial filters

The ancestor of spatial filtering, Foucault's knife edge method, can be analysed with the formalism introduced in this section. Fig. 10a shows the relevant quantities in the Fourier plane. In this arrangement all the diffracted light with $k>k_c$ is stopped, while all the light with $k<k_c$, including most of the undiffracted light, is allowed to pass and form an image in Σ'. The effect of the knife edge can be written as

$\tilde{B}''(k) = B'(k)\left[1-\tilde{E}(k)\right]$, (eq.38) where $\tilde{E}(k) = 1$ for $k > k_c$ and $\tilde{E}(k) = 0$ for $k < k_c$.

This produces a wavefield in the image plane given as

$B''(x) = \{[1+i\phi(x)]B(x)\}\otimes[\delta(x)-E(x)]$ (eq.39), where

$E(x) = FT^{-1}\{\tilde{E}(k)\} = \exp(ik_c x)[\delta(x)/2 + i/x]$.

Just as in the case of phase contrast we calculate the intensity interference terms for $\phi(x)=\delta(x-y)$ to obtain a wavenumber response:

$$h_i(x,y) = -i\{B(x)\otimes[\delta(x)-E(x)]\}B^*(x)\{\delta(x-y)-E(x-y)B^*(y)/B^*(x)\}+c.c. \quad \text{(eq.40)}$$

Since the knife is positioned such as not to significantly perturb the undiffracted light we can write

$\{B(x)\otimes[\delta(x)-E(x)]\}B^*(x) \cong B(x)B^*(x) = I_0(x)$ (eq.41) .

This leads to the following impulse response, evaluated at x=0:

$$h_i(u) = iI_0\left\{\frac{B^*(-u)E(u)}{B^*(0)} - \frac{B(-u)E^*(u)}{B(0)}\right\} \cong 2I_0\,\mathrm{Im}(E(u)) = I_0\frac{\cos(k_c u)}{u} \quad \text{. (eq.42).}$$

Since the impulse response is real and odd, the transfer function is imaginary and odd:

$$H_i(k) = iI_0\left\{\frac{\tilde{B}^*(k)\otimes\tilde{E}(k)}{B^*(0)} - \frac{\tilde{B}(-k)\otimes\tilde{E}(-k)}{B(0)}\right\} \quad \text{(eq.43).}$$

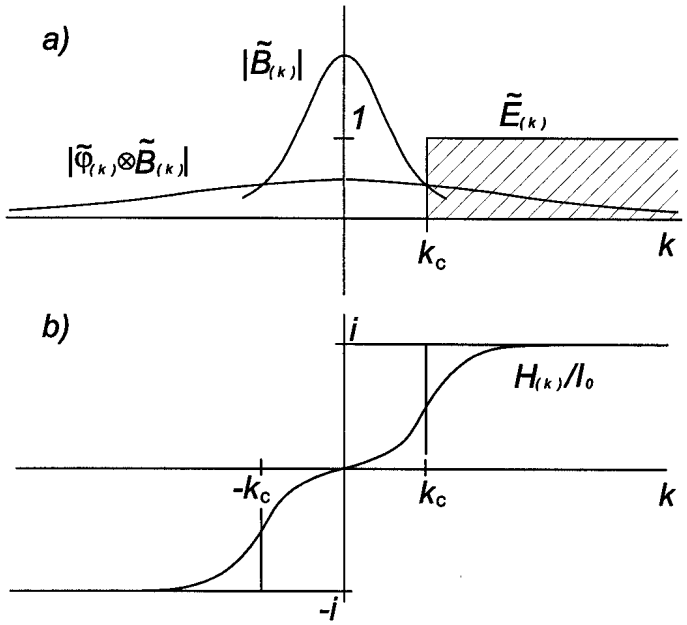

Fig.10 Fourier plane quantities and transfer function for the knife edge method.

Note that $\tilde{B}(\pm k) \otimes \tilde{E}(\pm k) \rightarrow B(0)$ for $k \rightarrow \infty$. If, as is usually the case in experimental situations, $\tilde{B}(k)$ can be taken to be both real and even, eq.43 further simplifies to (fig.10b):

$$H_i(k) = iI_0\left\{\frac{\tilde{B}(k) \otimes \left[\tilde{E}(k) - \tilde{E}(-k)\right]}{B(0)}\right\} \quad \text{(eq.44)}.$$

The impulse response and transfer function are depicted in fig.11d & d'(solid lines).

An improved version of Foucault's knife edge method consists in replacing the knife edge by a transparent blade causing a phase shift equal to π for all light diffracted at angles larger than k_c/k_0. This case is treated by setting $\tilde{E}(k) = 2$ (instead of 1) for $k > k_c$ and $\tilde{E}(k) = 0$ for $k < k_c$ in eq.38. Hence the impulse response and transfer function for the phase blade are therefore simply twice those of the knife edge. The corresponding transfer function is shown in fig.12d' (broken line).
Comparing figs 11b' and d' we note that for the same value of k_c the moduli of H_i are remarkably similar, in shape and absolute value, for the phase blade and phase contrast, indicating that both methods can extract the information contained in the transmitted beam equally well. However the fact that H_i is imaginary in the former case, as well as the oscillatory character of h_i, show that an image produced by a phase blade will in general be far more difficult to interpret that one obtained by phase contrast or using an interferometer.

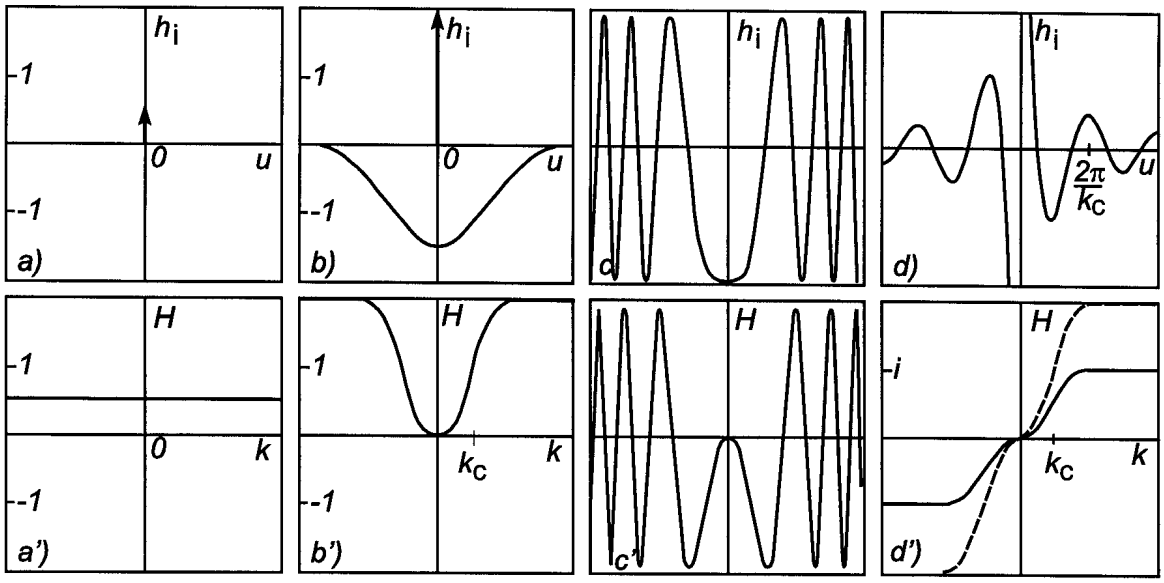

Fig.11 Impulse responses and transfer function of methods for measuring small phase shifts.

a), a') Interferometry

b), b') Phase Contrast

c), c') Scintillation

d), d') Knife edge and phase blade

4.5 Sensitivity

Since all methods can be compared on the basis of their transfer functions, we only need to treat the case of phase contrast, assuming photoamperic detectors which produce a photocurrent given by $j = Ae\eta\Phi$ where $\Phi = I/\hbar\omega$ is the photon flux onto the detector of area A and quantum efficiency η. In most circumstances, when the background intensity (I_0/γ^2 for phase contrast) is high enough, the main limitation for photoamperic detectors is due to shot noise (Teich 1968) with a noise power given by

$\left\langle j_n^2 \right\rangle = 2e\Delta f \times j = 2e^2 A\eta\Delta f\Phi$ (eq.45), where $\Delta f = \Delta\omega/2\pi$ is the bandwidth under consideration. The mean signal power for phase contrast is given by

$\left\langle j_s^2 \right\rangle = 4A^2e^2\eta^2\gamma^2\left\langle \phi^2 \right\rangle\Phi_0^2$ (eq.46), with $\Phi \cong \Phi_0 = I_0/\gamma^2$.

The signal-to-noise power ratio is then

$$S/N = \frac{2A\eta I_0\left\langle \phi^2 \right\rangle}{\hbar\omega\Delta f} \text{ (eq.47).}$$

Note that although the S/N ratio increases with illumination intensity, high intensities may require the direct light to be attenuated ($\gamma<1$) in order to avoid saturating the detectors. If this is not possible, the sensitivity will be limited by the maximum power tolerable on the detector.

The sensitivity limit (S/N=1) corresponds to

$\left\langle N_e^2 \right\rangle_{\min} = \frac{1.3\times10^4\Delta f}{\lambda^3 A\eta I_0}$ (eq.48) where $N_e = \int n_e dl$ is the electron line integrated density.

Although the wavelength dependence appears to favour the choice of far-infrared wavelengths, the mid-infrared offers far higher laser powers (tens of Watts) and somewhat more convenient detectors with quantum efficiencies in the range 20-70%. If a CO_2 laser (λ=10.6μm) and HgCdTe photoamperic diodes ($A\eta I_0\approx$1mW) are used the sensitivity limit corresponds to $\langle\phi^2\rangle^{1/2}=3\times10^{-6}$radians or $\langle N_e^2\rangle^{1/2}=10^{14}$ electrons/m^2 for Δf=1MHz. If these fluctuations are associated with effective integration lengths of a few cm, as is the case in many experiments (see exercises), this sensitivity limit corresponds to a local electron density fluctuation of $\Delta n_e\approx2\times10^{15}$ m^{-3} and to $\Delta n_e/n_e\sim10^{-4}$ for most current fusion research devices.

5) Fluctuation measurements using phase contrast on tokamaks

5.1 Instrumental setup

The phase contrast method has been used on three tokamaks (Weisen 1985,1988b), DIII-D (Coda and Porkolab, 1992, 1995) and recently on C-MOD, to study broadband turbulence, transient instabilities and radio-frequency driven waves. Fig.12 shows the phase contrast apparatus which was used on the TCA tokamak (R=61cm, a=18cm, B_T=1.5T) to measure kinetic Alfvén waves and plasma turbulence. It used a double-sided vertical optical "breadboard". An 8-Watt waveguide CO_2 laser and beam expansion optics were mounted on the rear side (not shown) and the imaging optics and detector were on the front side. The beam was expanded to a size of 23×5cm using an off-axis parabolic mirror with 190.5 cm focal length obtained by halving an inexpensive mirror for an astronomical telescope. The other halve , labelled P in fig.13, played the role of lens L1 in fig.8.

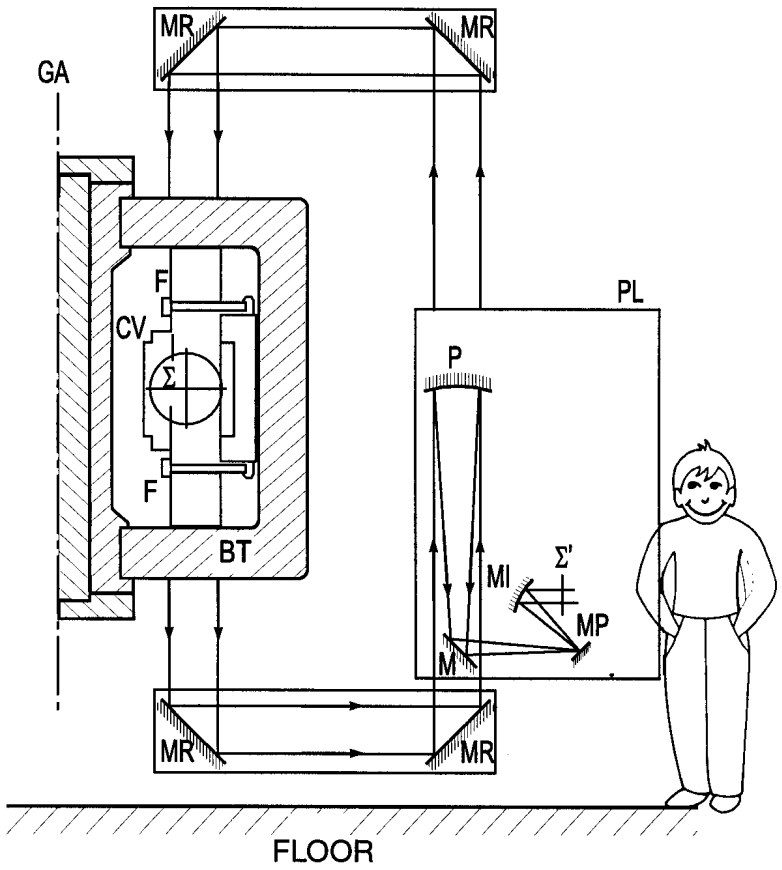

Fig.12 Optical arrangement for phase contrast on the TCA tokamak. PL optical table, Σ object plane at the plasma midplane, F vacuum window, CV vacuum chamber, BT toroidal field coil, GA major axis, P parabolic mirror (f=190.5cm), M flat mirror, MP phase mirror, MI imaging mirror (f=27cm), Σ' first image plane.

The beam was relayed to, and back from, the plasma by two sets of three flat mirrors, 45×7cm in size, which were mounted in rigid boxes at right angles to each other in a corner-cube arrangement. Only two mirrors are shown for simplicity. This arrangement provides immunity against rigid-body movements of the optical breadboard or any of the mirror boxes. As a result it was possible to suspend the upper box from the tokamak support frame, while the lower box and breadboard were standing on the floor. All three assemblies were independently vibration isolated. Without such passive vibration proofing, active feedback stabilization, as used by Coda and Porkolab (1992) on DIII-D, is necessary in order to keep the focal spot at the required position in the focal plane of mirror P.

The TCA tokamak vacuum vessel was initially equipped with elongated (23×3.6 cm clear aperture) composite NaCl windows (H.Ripper and H. Weisen 1987) with a thickness of 3.0 cm, which were later replaced by ZnS windows. These windows allowed access to more than half of the plasma poloidal cross section. Unfortunately on larger devices access to such a generous portion of the plasma cross section is very difficult

Phase mirrors (rather than phase plates) were obtained for both the TCA and the DIII-D experiments by evaporating a layer of aluminium onto flat steel mirror substrates, with thin flat brass ribbon of the required width (120-1050 μm for a diffraction limited spot size of 120μm) stretched across them. A final coating of gold further increased reflectivity. At the design incidence angle of 20^0, the 1.4μm deep groove produces the desired 90^0 phase shift between diffracted and direct light (fig.13). Contrast-enhanced phase mirrors were also produced, using ZnSe (γ=0.4) and BaF2 (γ=0.2) as substrates.

The light reflected from the phase mirror was collected by another off-axis paraboloid, M1 with focal length f=27cm on TCA, to obtain an image at Σ'. In the arrangement shown in fig.14 this image was not used directly, but relayed to Σ'' in a way suitable for the down-looking liquid-nitrogen cooled infrared photoconductive detector array shown. This linear array featured 30 elements, 250×250 μm in size and 50μm spacing between adjacent elements. The overall magnification was 1/19, allowing a full coverage of the outer half of a poloidal cross section.

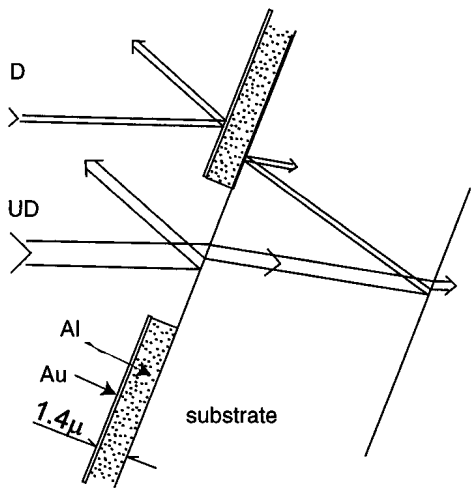

Fig.13 Phase mirror. UD undiffracted light, D diffracted light. The rays shown inside the substrate are for the case of dielectric substrates.

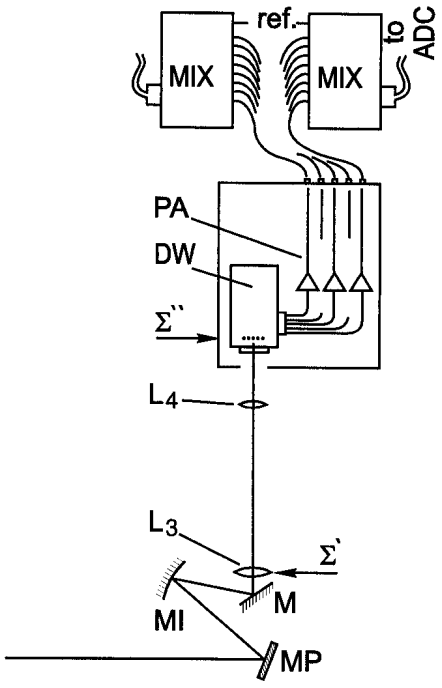

Fig.14 Detail of imaging optics with photoconductive detector array. Σ' first image plane as in fig 12, M flat mirror, MI first imaging mirror (f=27cm), L3 field lens made of BaF2 (f=35 cm) , L4 second imaging lens (f=10cm), Σ'' second image plane with 30-element detector array in nitrogen cooled dewar DW, PA preamplifiers (gain=4000), MIX mixers arrays for synchronous detection of fluctuations during radio frequency experiments

Performance tests and calibrations were performed in several ways; using sound waves from a loudspeaker, together with a calibrated sound meter to measure the pressure and hence density oscillations, by inserting thin Mylar plastic sheets to measure the step response and by direct measurements of the impulse response (Weisen 1988b). Only the latter will be presented here, since it relates directly to the theory presented in the previous sections. It can be shown (see exercise 2) that a narrow opaque bar produces nearly the same response as a narrow phase object. Hence a narrow metal bar scanned across the object plane produces a response which is proportional to the impulse response. Paradoxically, at the image of the bar the intensity is approximately doubled. Figure 15a shows the experimental impulse response obtained for a mirror with k_c=0.3 cm^{-1}. The transfer function, obtained by Fourier transformation, is shown on fig.15b.

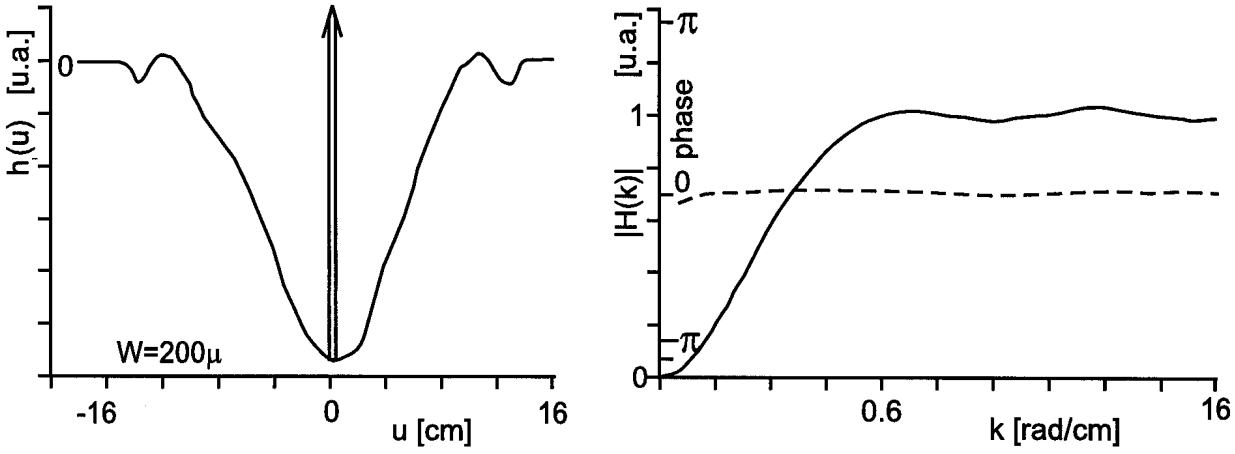

Fig.15 Experimentally measured impulse response (left) obtained using the opaque bar method and corresponding transfer function (right).

5.2 Applications

The main application of the diagnostic on TCA was to measure kinetic Alfvén waves produced in Alfvén Wave Heating experiments using external antennae at frequencies in the range 1.8-2.7 MHz (Weisen et al 1989b). This wave propagates radially inward from the shear Alfvén resonance layer. The signals from the detectors were synchronously amplified using the mixers sketched in fig.15. Fig.17 shows the (line integrated) wave amplitude profiles for (n,m)=(2,0) and for (1,1), as determined from the antenna phasings. The plasma wave phase profile seen in figs 17a and b is indeed characteristic of inward propagating waves which are (Landau) damped before they reach the plasma centre. The jumps by $\pm\pi$ seen in fig17c however reveal a standing wave pattern characteristic of a global eigenmode of the kinetic Alfvén wave, observed when conditions are such that the waves can propagate to the centre and are "reflected back". The dispersion properties of experimentally detected plasma waves can be used to provide further information on plasma parameters (Weisen et al 1989a).

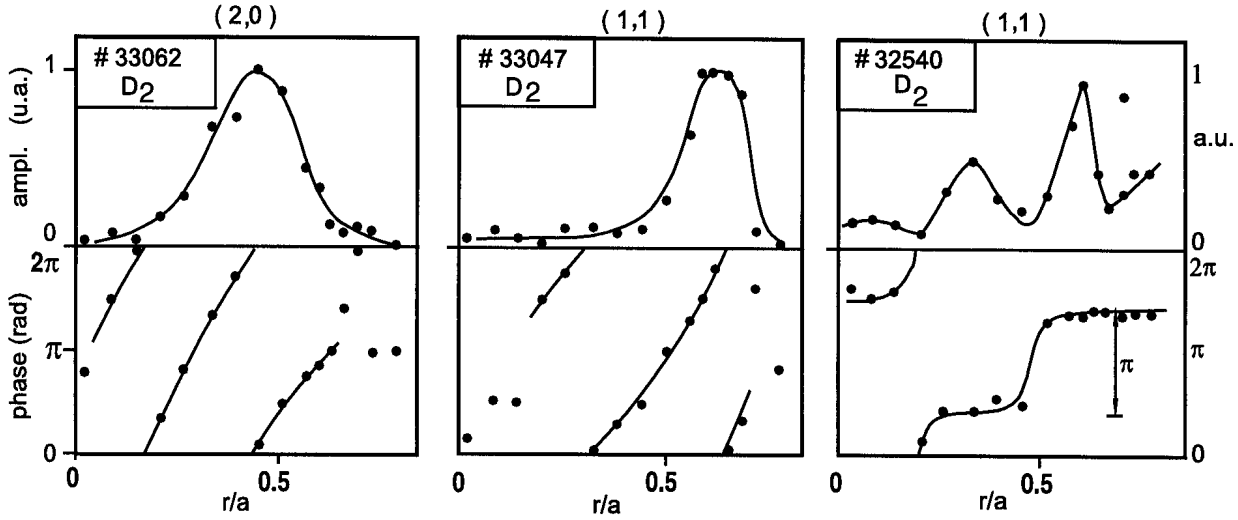

Fig.16 Radial wavepatterns of Kinetic Alfvén Waves in the TCA tokamak. Left and middle: (n,m)=(2,0) and (1,1) traveling waves. Right: (1,1) global oscillation

The investigation of plasma turbulence using imaging methods relies on correlation measurements similar to those used for probe measurements (Weisen 1988a, Wootton 1991). We may for instance compute the cross spectrum of the turbulent signals

$$p_{12}(\omega) = p(x,\Delta x,\omega) = \langle \phi^*(x,\omega)\phi(x+\Delta x,\omega)\rangle \quad \text{eq.49,}$$

using signals from two detectors (labelled 1 and 2) separated by a distance Δx. The argument ω means the component of the Fourier spectrum for frequency ω. In practice digitised, stationary signals are divided into N intervals of the same duration, their temporal Fourier spectra and finally the above averages are computed. If the turbulent medium is uniform the argument x in eq.49 is immaterial. The cross power can be normalised as

$$\gamma_{12}(\omega) \equiv \frac{p_{12}(\omega)}{\sqrt{p_{11}(\omega)p_{22}(\omega)}} \quad \text{(eq.50)}$$

and the coherence lengths as the distance Δx over which the coherence $|\gamma_{12}|$ drops from 1 to 1/e. In tokamak experiments drift wave turbulence is a universally observed feature. Fig.18 shows an

example of the coherence and the phase of the cross spectrum for drift wave turbulence in TCA at f=ω/2π=100kHz, at the maximum of the spectral power density. The coherence length is about 3cm, the mean wavenumber, obtained from the phase, about 1.5 cm^{-1}. To obtain a fully spectral representation the cross spectra are Fourier transformed with respect to u=Δx, to yield the power spectrum:

$$S(k,\omega) = \int p(u,\omega)\exp(-iku)du \text{ (eq.51)},$$

and the conditional spectrum:

$$s(k:\omega) = \int \gamma(u,\omega)\exp(-iku)du \text{ (eq.52)}.$$

A full power spectrum is shown in fig. 19 for a measurement on TCA and peaks near k=1.5 cm^{-1}, which is too low to allow spatial resolution with scattering methods of any wavelength for which the plasma is accessible to electromagnetic waves (Weisen et al 1988a). These power spectra are the same as those that could be obtained by multi-channel scattering diagnostics having the same large probe beam width for adequate wavenumber resolution at small wavenumbers. The measurement of plasma turbulence using these optical methods suffers two main drawbacks. The first is that the measurements usually have poor or no spatial resolution along the direction of propagation and hence provide a superposition of signals from regions with possibly very different behaviour, although sensible estimates of local properties are possible (see exercises). Scattering diagnostics using longer wavelengths can only provide spatial resolution for large enough wavenumbers, usually not however at the small wavenumbers at which the turbulent spectral power density is highest. The second is that their importance for transport cannot be deduced from the amplitude and spectra of the density fluctuations alone. Only diagnostics such as Langmuir probes (which are restricted to the plasma edge) or heavy ion probes can measure the local turbulent flux $\Gamma \propto \langle \tilde{n}\tilde{v}_r \rangle = \langle \tilde{n}\tilde{E}_\theta / B \rangle$, where $\tilde{v}_r$ is the fluctuating radial velocity, $\tilde{E}_\theta$ the fluctuating poloidal electric field, and B the magnetic field. (Wootton, 1991).

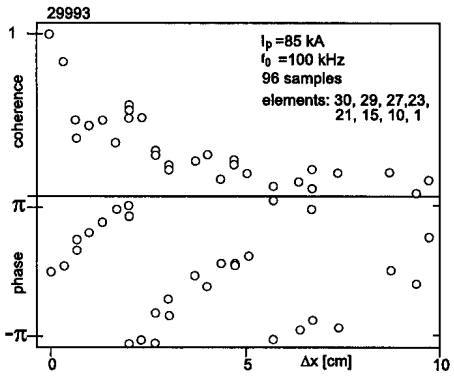

Fig.17 Autocorrelation function of plasma turbulence obtained from simultaneous cross-spectrum measurements at 8 different positions simultaneously.

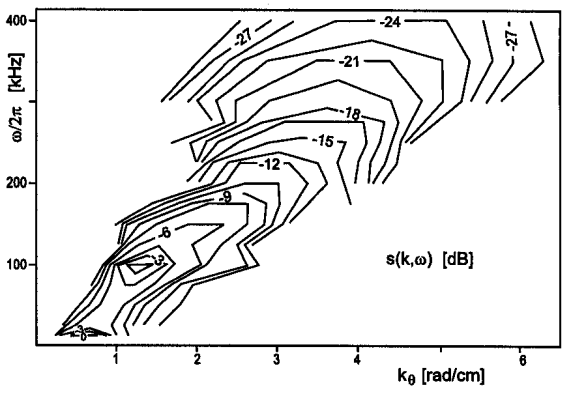

Fig.18 Power density spectrum obtained from correlation measurements near a central chord in TCA ($k \cong k_\theta$). The spacing of contour lines is a factor of 1.4.

6) Exercises

Exercise 1. Contrast enhancement

Derive the transfer function of phase contrast for $\gamma \neq 1$ (eq. 30b), by retracing the steps corresponding to equations 26-30, starting with the modified equation 25b.

Exercise 2. Effect of amplitude object on phase contrast system

Consider an object with an absorption $0 \leq \alpha \leq 1$:

$$B'(x) = [1 - \alpha(x)]B(x)$$

Calculate the resulting intensity change $\Delta I(x)$ resulting from the interference of terms which are linear in α with those which are independent of α, as well as the terms containing α^2. First consider a small opaque object such as a narrow bar with $\alpha(x)=1$ for $y-w/2<x<y+w/2$ and $\alpha(x)=0$ otherwise, where $w \ll D$, D being the width of the incident beam. Show that, paradoxically, at the position of the bar, the intensity is approximately doubled, i.e. $\Delta I \cong I_0$. The power necessary to build up this intensity spike is compensated by a reduction of intensity elsewhere in the beam. Show that this part is essentially described by the second term on the RHS of eq.27, with ϕ replaced by $-\alpha$, proving thereby that the impulse response of a phase contrast system can be measured using an opaque phase object. Now calculate the transfer function for weakly absorbing objects: $\alpha(x) \ll 1$, neglecting second order terms in α. Is the phase contrast system a high pass filter for amplitude objects, or is it a low pass filter?

Exercise 3. The ideal internal reference interferometer

In the previous sections we have learned how to calculate the transfer properties of spatial filtering methods given a particular optical set-up. We now wish to know what the transfer properties of a theoretically ideal imaging instrument are, one that would be limited only by basic physical principles and not by laboratory technicalities. To this effect we express the interaction with the phase object as giving rise to a diffracted component iD(x),

$$B'(x) = B(x) + iD(x)$$

where $D(x) = \phi(x)B(x)$ and we have assumed $\phi \ll 1$.

Conservation of energy implies $\|B\|^2 = \int B^*(x)B(x)dx = \|B\|^2$ where $\| \ \|$ designates, in a functional sense, the norm of B(x). What does conservation of energy imply for the diffracted component? Using the scalar product of B and D, decompose the function D into a component that is parallel in function space to B(x), i.e. $D_{\|}(x)=\eta B(x)$ and its perpendicular components $D_{\perp}(x)=D(x)-D_{\|}(x)$. Show that only $D_{\perp}(x)$ can contribute to producing intensity modulations as a result of the phase modulations ϕ. Now, defining an ideal instrument as one that makes use of all of the $D_{\perp}$ wavefield, calculate $\Delta I(x) = B^*(x)D_{\perp}(x) + c.c$, compare with equation 27 and following the procedure from eq.27 to 30, calculate the impulse response and the transfer function. Note in particular, that the weighting function, with respect to which $\phi(x)$ is measured, is the normalized intensity profile $B^*(x)B(x)$.

Exercise 4. General limitations at small wavenumbers for internal reference methods

Taking the considerations in exercise 3 a little further, we may ask ourselves what maximum power we may obtain from any diffraction process, if we use the transmitted beam as a local oscillator, be it in the near field or in the far field. Since the scalar products of optical wavefields are conserved during propagation we only need to evaluate the relevant quantities after transmission through the phase object at Σ. The largest possible power is obtained by producing interference between the $D_\perp$ wavefield and the incident wavefield B, i.e

$\Delta P \le 2\|D_\perp\|\|B\| \le 2\|D\|\|B\|$. Provide an expression for the maximum homodyning efficiency $\varepsilon_{max} = \|D_\perp\|/\|D\|$, first for arbitrary ϕ, then obtain $\varepsilon_{max}(k)$ by setting $\phi(x)=\phi_0\exp(ikx)$. Finally consider a Gaussian beam, $B(x)=\exp(-x^2/2w^2)$ and show that $\varepsilon_{max}(k)=\{1-\exp(-k^2w^2/2\}^{1/2}$.

Exercise 5. Shot noise from an ideal photodiode

When the photocurrent from a photodiode is large enough the dominant source of noise is due to photoelectron (Poisson) statistics. Derive equation 45 for shot noise, associating an effective integration time $\tau=(2\Delta f)^{-1}$ with the bandwidth Δf.

Exercise 6. Effective integration length in a turbulent medium.

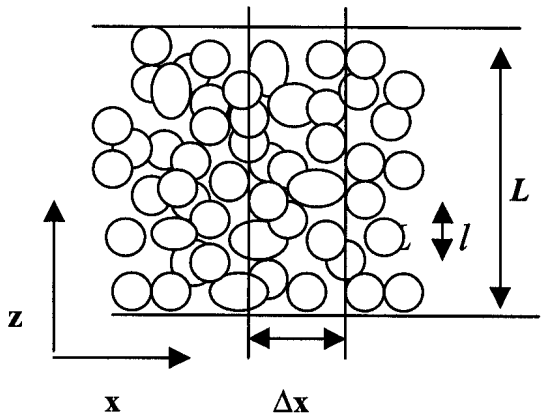

A plane wavefront propagating in direction z enters a homogeneous turbulent refractive slab of thickness *L*. The turbulence is characterized by a coherence length *l* in the direction of propagation and fluctuations with average amplitude n^*_{rms}. Calculate the variance of the resulting phase upon exit from the slab using a random walk argument. Show that the propagation through the slab is associated with an effective integration length $L_{eff} = \sqrt{lL}$.

Exercise 7. Line integrated correlation measurements.

Considering the geometry of exercise 6, show that the autocorrelation function for the line-integrated turbulent fluctuations may be written as

$$\overline{\Gamma}(\Delta x,\Delta t)=\iint\Gamma(\Delta x,\Delta z,\Delta t)dzd\Delta z=L\int\Gamma(\Delta x,\Delta z,\Delta t)d\Delta z$$

where $\overline{\Gamma}(\Delta x,\Delta t)=\left\langle\tilde{N}(x,t)\tilde{N}(x+\Delta x,t+\Delta t)\right\rangle$, $\Gamma(\Delta x,\Delta z,\Delta t)=\left\langle\tilde{n}(x,z,t)\tilde{n}(x+\Delta x,z+\Delta z,t+\Delta t\right\rangle$ and $\tilde{N}(x,t)=\int\tilde{n}(x,z,t)dz$ and $\left\langle\tilde{n}(x,z,t)\right\rangle=0$.

How can the local autocorrelation function Γ be reconstructed from a measurement of $\overline{\Gamma}$ in the case of homogenous isotropic turbulence? Using a suitable definition for the coherence length l_z, give an alternative derivation for the result of exercise 6, namely $\left\langle\left|N(x,t)\right|^2\right\rangle=l_zL\left\langle\left|n(x,z,t)\right|^2\right\rangle$.

Exercise 8. Line integral through a spherical wavefront

Consider a spherical (or cylindrical) refractive wave of the form $\tilde{n}(r,t)=f(r)\exp i(kr-\omega t)$, such as produced by a loudspeaker or a radially propagating plasma wave. Show that for a sufficiently slowly varying envelope factor f(r), such that df(r)/dr<<kf(r), and r>>Λ, the line integral can be approximated by

$\tilde{N}(x,t)=\int\tilde{n}(x,z,t)dz\cong f(x)\sqrt{\Lambda x}\exp i(kx-\omega t+\pi/4)$, where $\Lambda=2\pi/k$ is the refractive wavelength.

Answers and hints to some of the exercises

Exercise 2

The answer is

$$\Delta I(x)=\alpha^2(x)B^2(x)-\{C(x)\otimes[\alpha(x)B(x)]\}\{4[C(x)\otimes B(x)]-2B(x)\}$$
$$-2\alpha(x)B(x)\{C(x)\otimes[\alpha(x)B(x)]\}$$
$$+2\alpha(x)B(x)\{C(x)\otimes B(x)\}-2\alpha(x)B^2(x)$$
$$+2\left|C(x)\otimes[\alpha(x)B(x)]\right|^2$$

The two first RHS terms correspond the RHS of eq.27, since $C(x)\otimes B(x)\cong B(x)$, whilst the fourth and the fifth approximately cancel, the sixth being negligible for small or weakly absorbing objects. For a narrow opaque object the first term causes a local doubling of the intensity, the second an overall reduction, and the third another modest local reduction. For weak absorption (α<<1) the third term is dominant and corresponds to a spatial low pass filter with cutoff wavenumber k_c.

Exercises 3 and 4

Details may be found in H.Weisen 1986 (appendix).

Exercise 6

The problem corresponds to that of a random walk with m=L/l steps of amplitude s=$k_0 l n^*$. The average walk amplitude for random walk being S=$sm^{1/2}$, the average phase perturbation is $\phi_{rms}=k_0(Ll)^{1/2}n^*_{rms}$.

Exercise 7

Details may be found in H. Weisen et al (1988a, appendix). In the case of homogeneous isotropic turbulence the local autocorrelation function can be retrieved by an Abel inversion on the line integrated autocorrelation function. The same applies to the cross-spectra.

Exercise 8

Hint: Use the following second order approximation: $r=\sqrt{x^2+z^2}\cong\left|x+z^2/2x\right|$ in the expression of the refractive wave phase, or, equivalently, use the following approximation provided by the method of steepest descent: $\int_{\Re}\exp i\{n(z)\}dz\cong\sqrt{2\pi\left|\frac{\partial^2 n}{\partial n^2}\right|^{-1}_{z=0}}\exp i\{n(0)\pm\pi/4\}$ the +sign being applied when $\left|\frac{\partial^2 n}{\partial n^2}\right|_{z=0}<0$, the – sign otherwise.

Acknowledgement

I'm highly indebted to Professor Alexander Ivanov of the Budker Institute of Nuclear Physics for having translated this work into the Russian language. This work was partly supported by the Swiss National Funds for Scientific Research.

References

Brower D.L. et al, Phys.Rev.Lett 54 (1985) 689

Brower D.L, W.A. Peebles and Luhmann N.C, Jr, Nuclear Fusion 27 (1987) 2055

Coda S. and Porkolab (1992) Rev. Sci. Instrum. 63, 4974

Coda S. and Porkolab (1995) Rev. Sci. Instrum. 66, 454

Gaskill G. *"Linear Systems, Fourier Transforms and Optics"*, (1978), Wiley, New York.

Holzhauer E. and Massig J.H., Plasma Physics 20 (1978) 867

Hugenholtz C.A.J. and Meddens B.J.H., Rev. Sci. Instrum 53 (1982) 171

Jackson J.D. *"Classical electrodynamics"*, 2nd edition, John Wiley and sons, 1975

Jahoda F.C. and Sawyer G.A. in *"Methods of Experimental Physics"*, Vol 9B (1971), edited by Lovberg R.H. and Griem H.R., Academic Press

Mazzucato E., Phys.Rev.Lett 36 (1976) 792

Presby H.M. and Finkelstein D., Rev.Sci.Instrum 38 (1967) 1563

Slusher R.E. and Surko C.M. Phys.Fluids 23 (1980) 472

Teich M.C. *"Infrared Heterodyne Detection"*, Proc.IEEE 56 (1968) 37

Thon F. in Electron Microscopy in Material Science (1971) edited by V. Valdré, Academic Press, 571

TFR group and Truc A., Plasma Phys.Contr.Fusion 26 (1984) 1045

Vasil'ev L.A. *"Schlieren Methods"*,1971, Israel program for scientific translations. Distributed by Keter Publishers Ltd, London

Véron D., in Infrared and Millimeter waves, vol (1979) , p67
edited by K.J. Button, Academic Press, New York

Weisen H., Infrared Physics 25 (1985) 543

Weisen H., Plasma Physics and Controlled Fusion 8 (1986), 1147

Weisen H and Ripper H., Infrared Phys. 27 (1987), 375

Weisen H., Hollenstein Ch and Behn R., Plasma Physics and Controlled Fusion (1988a), 293

Weisen H., Rev.Sci.Instrum. 59 (1988b) 1544

Weisen H. et al, Phys.Pev.Lett 62 (1989a) 434

Weisen H. et al. Phys.Rev.Lett 63 (1989b) 2476

Wolter H. (1956) in Handbuch der Physik, Band XXIV, Grundlagen der Optik, Springer Verlag, 555

Wootton A. in *"Diagnostics for contemporary fusion experiments"*, Course and workshop, 1991, Varenna, Italy

Young P.E. et al, Rev. Sci. Instrum 56 (1985) 81

Zernike F., Mitteilungen des Naturkundigen Labors, Universität Groningen, Haag 1 (1934) 43.

Zernike F., Zeitschrift für technische Physik 16 (1935) 454